Talanta 232 (2021) 122427

Contents lists available at ScienceDirect

Talanta

journal homepage: www.elsevier.com/locate/talanta

# Visual-afterglow dual-mode immunochromatographic strip for 17β-estradiol detection in milk

Yi Zhang [a,b,c,*], Lingling Wang [a,b,c], Wen-Long Wang [a,b,c], Cheng Yang [a,b,c], Yongwei Feng [d], Xueli Shi [e,**]

[a] State Key Laboratory of Food Science and Technology, Jiangnan University, Wuxi, 214122, Jiangsu, China
[b] International Joint Laboratory on Food Safety, Jiangnan University, Wuxi, 214122, Jiangsu, China
[c] Institute of Analytical Food Safety, School of Food Science and Technology, Jiangnan University, Wuxi, 214122, Jiangsu, China
[d] Wuxi Institute of Food Control, Wuxi, 214100, Jiangsu, China
[e] Shijiazhuang City Maternal and Child Health Hospital, Shijiazhuang, 050051, Hebei, China

ARTICLE INFO

*Keywords:*
Afterglow
Dual-mode
Immunochromatographic strip
Estradiol
Milk

ABSTRACT

The continuous intake of 17β-estradiol (E2) residue from animal-derived food may pose a threat to the health of consumers, so the rapid screen and detection of E2 is very necessary. Although visual immunochromatographic strip (ICS) has played a great role in food safety control such as the screen of many food contaminants, it cannot meet the requirements for E2 detection due to the insufficient sensitivity of traditional visual ICS and the low concentration range of estrogen in food. Here, we developed a dual-mode ICS strategy to achieve rapid and highly sensitive detection of E2. Based on the visual detection mode of a competitive ICS, the afterglow detection mode working in fluorescence resonance energy transfer mechanism was introduced by using the afterglow particles (APs) as energy donor and gold nanoparticles (AuNPs) as energy acceptor. In this method, large APs of micron size with superior afterglow were applied as the test zone-fixed fluorescence signal source, thus the contradiction between migration and afterglow characteristics was skillfully resolved. In addition, a 6 W UV lamp was used as the light source to excite APs, and a smartphone was used to capture an image of 0.5 s after the UV light was turned off to effectively remove the autofluorescence from the strips and improve the signal-to-noise ratio. The limit of detection of this afterglow mode was 0.5 ng/mL, twenty times more sensitive than that of visual mode (10 ng/mL). The strategy has been successfully applied to the detection of estradiol in milk and verified by HPLC–FLD.

## 1. Introduction

17β-Estradiol (E2) is a natural substance with strong biological activity in estrogens regulating reproduction and cardiovascular functions. However, when the amount of E2 accumulated through food and drinking water exceeds the threshold of E2 in human body, it will disrupt the endocrine balance, induce disease and even affect reproduction [1,2]. In 2002, announcement No. 176 of the Ministry of Agriculture of China clearly proposed the banning of using sex hormones including E2 in animal drinking water and feed. Although the Codex Alimentarius Commission and China's national food safety standards stipulate that E2 cannot be detected in feed, some farmers still utilize it to increase production, resulting in the residue of E2 in animal-derived food. Currently, E2 has been mostly detected by some methods including HPLC [3], GC [4], electrochemical (EC) sensor [5], and surface enhanced Raman spectroscopic (SERS) sensor [6], which are sensitive enough to detect E2 at ng/mL level or below. Whereas, rapid, cheap and sensitive detection methods for E2 are of great urgency for on-site testing in food market and food industry. However, HPLC and GC requires professional operators and could not be used in on-site detection. EC-based sensors and SERS-based sensors were time-consuming for sample preparation and detection process.

Immunochromatographic strip (ICS), a paper-based rapid detection technology, boasts the advantages of low cost and easy operation to be an ideal choice for on-site detection in clinical diagnosis [7], food safety [8], and environmental monitoring [9]. E2 has also been detected by

* Corresponding author. State Key Laboratory of Food Science and Technology, Jiangnan University, Wuxi, 214122, Jiangsu, China.
** Corresponding author.
*E-mail addresses:* zhangyijnu@jiangnan.edu.cn (Y. Zhang), shixueli1126@126.com (X. Shi).

https://doi.org/10.1016/j.talanta.2021.122427
Received 20 January 2021; Received in revised form 8 April 2021; Accepted 10 April 2021
Available online 4 May 2021

some ICS methods [10–12]. Gold nanoparticles (AuNPs) are used as the signal probe for most ICS because of its visible and obvious color by naked eyes, however, its low sensitivity limits its application in the detection of trace substances [13,14]. Therefore, many strategies, such as analyte concentration amplification before analysis [15,16], amplification of the AuNPs color signal [17], strip structure improvement [18] and membrane chemical modification [19], have been developed to improve the sensitivity of ICS.

Luminescent materials, such as silica particles encapsulated organic fluorescent dyes or europium coordination compounds [20–22], quantum dots [23,24], and up-conversion nanoparticles [25,26] etc. could be used as more sensitive signal probes than AuNPs. However, the luminescence signals from probes are subjected to interference of autofluorescence from nitrocellulose (NC) membrane, the separation membrane of ICS, or may need expensive laser of high power as excitation light source. Different from these luminescence signals, afterglow particles (APs) could emit persistent luminescence after ceasing excitation by UV-lamp and avoid the interference from NC membrane. It is worth mentioning that the afterglow time of APs synthesized by high-temperature solid-phase synthesis is longer than that of APs synthesized by other methods, because high-temperature sintering can increase the number of inherent thermal defects in long persistent phosphors and improve the afterglow performance. However, high calcination temperature will result in micron-sized particles that are too large to migrate across the strip [27].

Here, we skillfully resolved the contradiction between migration and afterglow characteristics by fixing the large bright APs at the test zone on the strip and established a visual-afterglow dual-mode ICS for E2 detection. The visual mode ICS was a classic competitive strategy, whereas the afterglow mode was based on fluorescence resonance energy transfer (FRET) principle, using E2-BSA-coupled afterglow particles (E2-BSA-APs) as the test zone fixed energy donor and AuNPs-labeled antibody as mobile energy acceptor. After ceasing the excitation, our afterglow material on ICS kept emitting for seconds. The unique optical characteristic enabled detection without in-situ excitation and to avoid the interference of autofluorescence and scattered light from complex substrates. In this work, the afterglow signal was collected by smart phone time-gated imaging, with no need of advanced optical signal detection device working in a time-resolved manner. In addition, dual signals also increase the accuracy and sensitivity of the results. Afterglow signal is positively correlated with E2 concentration, which is beneficial to obtain LOD from weak afterglow signals when there is a small amount of E2. We applied the strategy to the detection of E2 in milk.

## 2. Experimental section

### 2.1. Chemicals and reagents

Tetraethyl orthosilicate (TEOS, 96%), dimethyl sulfoxide (DMSO), Tween-20, sucrose, N-hydroxysuccinimide (NHS), 1-ethyl-3-(3-dimethylaminopropyl) carbodiimide hydrochloride (EDC·HCl), $HAuCl_4{\cdot}3H_2O$, bovine serum albumin (BSA), E2 were purchased from the Sinopharm Chemical Reagent Co., Ltd. (Shanghai, China). bisphenol A (BPA), estrone (E1), diethylstilbestrol (DES), estriol (E3), trisodium citrate dihydrate were purchased from Aladdin (Shanghai, China). Mouse anti-E2 monoclonal antibody (mAb) and goat anti-mouse secondary antibody were purchased from Shanghai Yuduo Biotechnology Co., Ltd. (Shanghai, China). Afterglow particles (APs) used in all ICSs were purchased from Hangzhou Zhicheng Technology Development Co., Ltd. (Hangzhou, China). The materials of the ICSs, including sample pads, absorbent pads, NC membranes and polyvinylchloride backing cards, were purchased from the Jieyi Biotechnology Co., Ltd. (Shanghai, China). Ultrapure water was purchased from Wahaha group Co. (Hangzhou, China). Methanol and acetonitrile of HPLC grade were purchased from Fisher Chemical (Shanghai, China). 10 mM phosphate-buffered saline (PBS) composes 4 g NaCl, 1.49 g $Na_2HPO_4{\cdot}12H_2O$, 0.12 g $KH_2PO_4$ and 500 mL ultrapure water, adjust to pH 7.4 or 6.0 as required.

### 2.2. Instrumentation

The size and morphology of the AuNPs were determined by a JEM-2100 HR transmission electron microscope (TEM, JEOL Ltd., Japan) at 200 kV. UV–vis absorption spectra were measured on a Shimadzu UV-2550 UV–vis spectrophotometer (Shimadzu, Japan). The phosphorescence spectra of APs were measured on a F-7000 fluorescence spectrometer (Hitachi, Japan). Zeta potential measurements were performed on a Nano-ZES Zetasizer system (Malvern, UK). Mass spectra of E2 and E2-CME were taken on a QTRAP 4500 ESI mass spectrometer (AB SCIEX, USA) with a negative ion mode and those of BSA and E2-BSA were performed on an Autoflex III MALDI-TOF-MS (BRUKER Ltd, Germany) with a positive ion mode. X-ray diffraction (XRD) pattern was performed on D2 PHASER powder diffractometer with a CuKα radiation source (Bruker, Germany). The morphology, elemental mapping and energy dispersive X-ray spectra (EDS) of the APs were performed on SU8010 scanning electron microscope (SEM, HITACHI Ltd, Japan). Fourier transform infrared (FT-IR) spectra were performed on Nicolet IS10 FT-IR spectrometer (Nicolet, USA). HPLC–FLD experiments were used as verification method and performed on a Waters E2695 separation module with a 2475 FLR detector (Milford, MA, USA). The separations were achieved on an XSelect® HSS C18 column (5 μm particle, 250 mm × 4.6 mm) purchased from Waters (Milford, MA, USA).

### 2.3. Synthesis of E2-BSA conjugates

The E2-BSA conjugates were processed according to the reported methods with some modifications [11,12]. 100 mg E2 and 500 mg KOH in DMSO were stirred for 10 min, and 100 mg bromoacetic acid was added for another 2 h reaction. Then ice cold water was added to stop reaction and ethyl acetate extraction to clean up unreacted E2. After acidification, white precipitate was produced, filtered, rinsed with distilled water to pH 7, and vacuum-freeze dried. 6.6 mg of the product E2-carboxymethyl ether (E2-CME), 6 mg of NHS, 7 mg of EDC·HCl in DMSO were stirred for 2 h and then 30 mg BSA in 50 mM carbonate-bicarbonate buffer (pH 9.6) was added for another 12 h reaction. The product E2-BSA was dialyzed against PBS (10 mM, pH7.4) and stored at −20 °C.

### 2.4. Synthesis of E2-BSA-APs

APs were modified referring to literature method [28–30]. 30 mg of APs was dispersed in 5 mL of anhydrous ethanol with ultrasonic dispersion for 5 min, then 0.13 mL of TEOS in ethanol-water (4:1, v/v) was added and bath sonicated for 5 min. Aqueous ammonium hydroxide (28–30%, 0.5 mL) was added, and sonicated for 30 min before being placed on the rotator at room temperature to process silica encapsulation for 7.5 h. The product was centrifuged at 10,000 rpm for 10 min, washed three times with anhydrous ethanol and vacuum dried, thus APs-$SiO_2$ was obtained.

To synthesize APs-COOH, the obtained APs-$SiO_2$ (50 mg) was ultrasonically dispersed in 25 mL water for 10 min and carboxyethylsilanetriol sodium salt (CES) was added dropwise following by 24 h reaction at room temperature. The product was centrifuged at 10,000 rpm for 10 min, washed with water and anhydrous ethanol, and vacuum dried at 37 °C.

We conjugated APs-COOH with E2-BSA by the active ester method [31]. 1 mg APs-COOH, 2 mg EDC·HCl and 5 mg NHS was ultrasonically dispersed in 1 mL PBS (10 mM, pH 6.0) and stirred for 2 h at room temperature. The mixture was centrifuged (6000 rpm, 6 min), washed and re-dispersed in 0.5 mL PBS (10 mM, pH 7.4). 0.5 mL E2-BSA (1 mg/mL) was added, stirred overnight, and collected by centrifugation (6000 rpm, 6 min, 4 °C). The product E2-BSA-APs was washed and

dissolved in 0.5 mL PBS (10 mM, pH 7.4) for use.

In order to verify the migration properties of the large APs, they were dispersed in PBS buffer (10 mM, pH 7.4) at a concentration of 2 mg/mL, and 1 μL of this dispersion was spotted on the NC membrane, ~0.5 cm to the sample pad. Immediately added 10 μL running buffer (10 mM PBS, 10% sucrose, 8% BSA, 1% Tween-20, pH 7.4), the running buffer flowed through the spot of APs and stopped before reaching the absorbent pad. Marked the front line of the running buffer with a pencil and took photos under the UV lamp after drying.

### 2.5. Synthesis of AuNPs-labeled anti-E2 mAb (AuNPs-mAb)

AuNPs were prepared using the trisodium citrate reduction method with slight modification [32]. 3 mL of 1% (w/w) freshly dissolved trisodium citrate was added into 100 mL of boiled $HAuCl_4$ aqueous solution (1/10,000, w/w). Keep heating and stirring for another 10 min and then naturally cooled down to room temperature under stirring. The prepared AuNPs solution was made up to 100 mL with pure water, filtered with a 0.45 μm polyethersulfone filter, and stored at 4 °C before use.

The AuNPs-antibody conjugate (AuNPs-mAb) was prepared as reported [11]. 1 mL AuNPs were finally dispersed in 0.05 mL buffer after turning into AuNPs-mAb.

### 2.6. AuNPs-FQ-ICS construction

Dual-mode ICSs were constructed by dropping 1 μL 2 mg/mL E2-BSA-APs as test (T) zone and 0.5 μL 0.1 mg/mL goat anti-mouse IgG as control (C) zone, following by drying at 37 °C for 30 min.

### 2.7. Sample analysis

Milk sample (10 mL) was adjusted to pH 4.5 by 5% HCl and centrifuged (10000 rpm) for 15 min to precipitate protein. Then the supernatant was adjusted to pH 7.4 by 5% NaOH and centrifuged (10000 rpm) for 15 min again. Different concentrations of E2 were added into the supernatant to bring a final concentration of E2 to 0 ng/mL, 1 ng/mL and 10 ng/mL.

40 μL sample solution, 5 μL of AuNPs-mAb and 10 μL of running buffer (10% sucrose, 8% BSA, 1% Tween-20, 10 mM PBS, PH 7.4) were mixed and incubated for 5 min and then ICSs were inserted into the mixture and run for ~15 min. For afterglow analysis, the strips were excited under a UV lamp of 254 nm, and then taking photos in continuous shooting mode since the light turned off. For each sample, the total assay time was about 50 min from sample preparation to data collection.

## 3. Results and discussion

### 3.1. Characterization of E2-BSA and E2-BSA-APs

E2-BSA conjugate was synthesized according to the chemical reactions shown in Fig. 1a. The intermediate E2-CME was identified by both HPLC–FLD and ESI MS. The liquid chromatogram of E2 and $BrCH_2COOH$ conjugating production revealed a new peak with the retention time of 5.2 min, slightly shorter than that of E2 (5.5 min) (Fig. 1b) and in their mixture they kept their own migration times, indicating the production of a new compound. The product was further analyzed by ESI mass spectrometry. The ion at *m/z* 329.00 was attributed to $[M - H]^-$ ion of E2-CME, with a difference of *m/z* 57.80 corresponding to a loss of a H and a gain of $–CH_2COOH$, comparing with $[M - H]^-$ ion of E2 (*m/z* 271.20) (Fig. 1c). The MALDI-TOF MS was used to verify the production of E2-BSA and calculate the binding ratio of E2 to

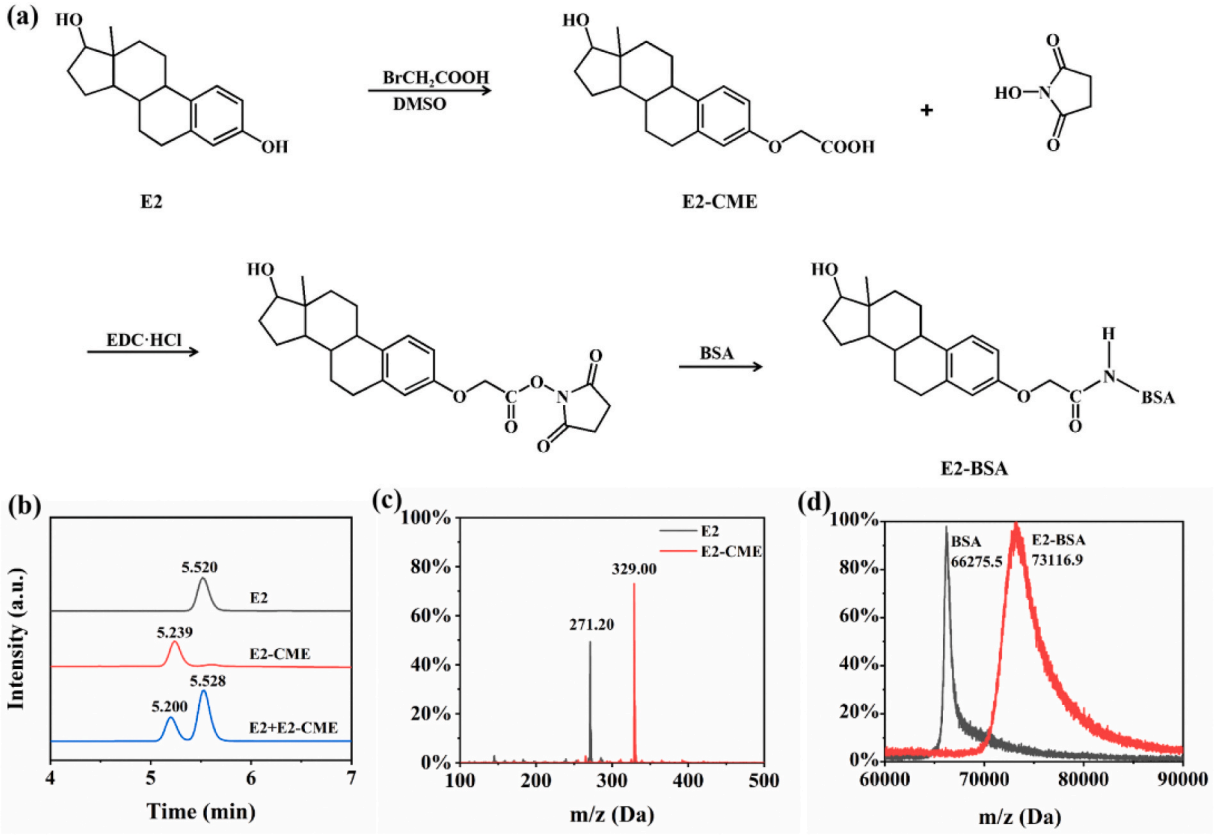


**Fig. 1.** (a) Mechanism of E2-BSA synthesis. (b) Liquid chromatograms of E2, E2-CME and their mixture. (c) ESI mass spectra of E2 and E2-CME taken at negative mode. (d) MALDI-TOF mass spectra of BSA and E2-BSA taken at positive mode.

BSA [12]. The mass spectrum of BSA peaked at *m/z* 66275.5, while the peak of E2-CME and BSA conjugating product shifted to larger *m/z* 73116.9, with an increase of *m/z* 6841, about twenty-one times of the molecular weight of E2-CME, therefore the conjugation ratio of E2-CME to BSA was about 21:1 (Fig. 1d).

We chose $SrAl_2O_4$: Eu, Dy as the afterglow material as this material exhibits a very bright visible afterglow, greatly exceeding that of any other materials known to date [33]. The host material $SrAl_2O_4$ is chemically stable and a large number of defects in its crystal structure can absorb photons, meanwhile, the doped Eu are the emission center and the doped Dy can further improve the intensity and prolong the duration of the afterglow. According to the supplier's claim, the APs we purchased were obtained by high temperature solid phase reaction, and we characterized their morphology and chemical composition. The APs were large particles in micron size (Fig. 2a), with hexagonal $SrAl_2O_4$ crystal phase (JCPDS card numbers 34–0379) (Fig. 2b). The constituent elements were Al, Sr, O, Eu (1.4 wt%) and Dy (0.1 wt%) (Fig. 2c and d).

E2-BSA was then conjugated with APs according to the procedures shown in Fig. 3a and the products were characterized by both zeta potential and FT-IR spectroscopy after each modification step. The zeta-potential of APs decreased from +4.3 mV to −16.7 mV (APs-$SiO_2$) after silica shell functionalization, and a further decrease to −25.5 mV (APs-COOH) was found after carboxyl modification (Fig. 3b). The conjugating of E2-BSA with APs-COOH also led to a zeta-potential decrease to −39.8 mV (E2-BSA-APs). Theoretically, the greater the absolute value of the particles' zeta-potential, the more stable the material is in aqueous solution. Thus, the results of zeta-potential characterization indicated not only the success of each reaction but also a new product with better stability after each modification step.

According to the FT-IR spectrum, APs−COOH displayed strong absorption band of O–Si–O at 1097 $cm^{-1}$, absorption band of the C═O stretching vibration at 1647 $cm^{-1}$ and free OH at 3550 $cm^{-1}$, respectively (Fig. 3c). After E2-BSA functionalization, E2-BSA-APs exhibited all the peaks of E2-BSA, revealing the successful conjugation.

### 3.2. Characterization of AuNPs and AuNPs-mAb

The prepared AuNPs were 15–20 nm in diameter, with uniform spherical shape (Fig. 4a) and a maximal absorption peak at 520 nm (Fig. 4b). After conjugating with anti-E2 mAb, the spectra showed two absorption peaks, one at 278 nm (antibody protein) and the other at 525 nm, a slightly red shift comparing with that of unmodified AuNPs possibly due to the coupling (Fig. 4b). The zeta potential increased from −35.1 mV (AuNPs) to −21.1 mV (AuNPs-mAb) (Fig. 4c).

### 3.3. Test principle

A schematic diagram of the visual-afterglow dual-mode ICS is presented in Fig. 5a. For negative samples, AuNPs-mAb can be captured by E2-BSA-APs at T zone due to the interaction between E2-BSA on APs and anti-E2 mAb on AuNPs. The T-zone captured AuNPs will not only show obvious red color, but also quench the afterglow of APs due to a fluorescent resonance energy transfer (FRET) from APs to the captured AuNPs, showing a dark red visual signal and a non-luminous afterglow signal, respectively. For positive samples, E2 in samples will compete with E2-BSA-APs on T zone to bind with AuNPs-mAb, resulting in the color of T zone to weaken or even disappear and also lighted afterglow because of less FRET. The minimum E2 concentration required to completely discolor T zone is the limit of detection (LOD) of visual mode, whereas that required to light up the afterglow of APs at T zone is LOD of afterglow mode.

According to the luminescence decay curve, the afterglow of APs

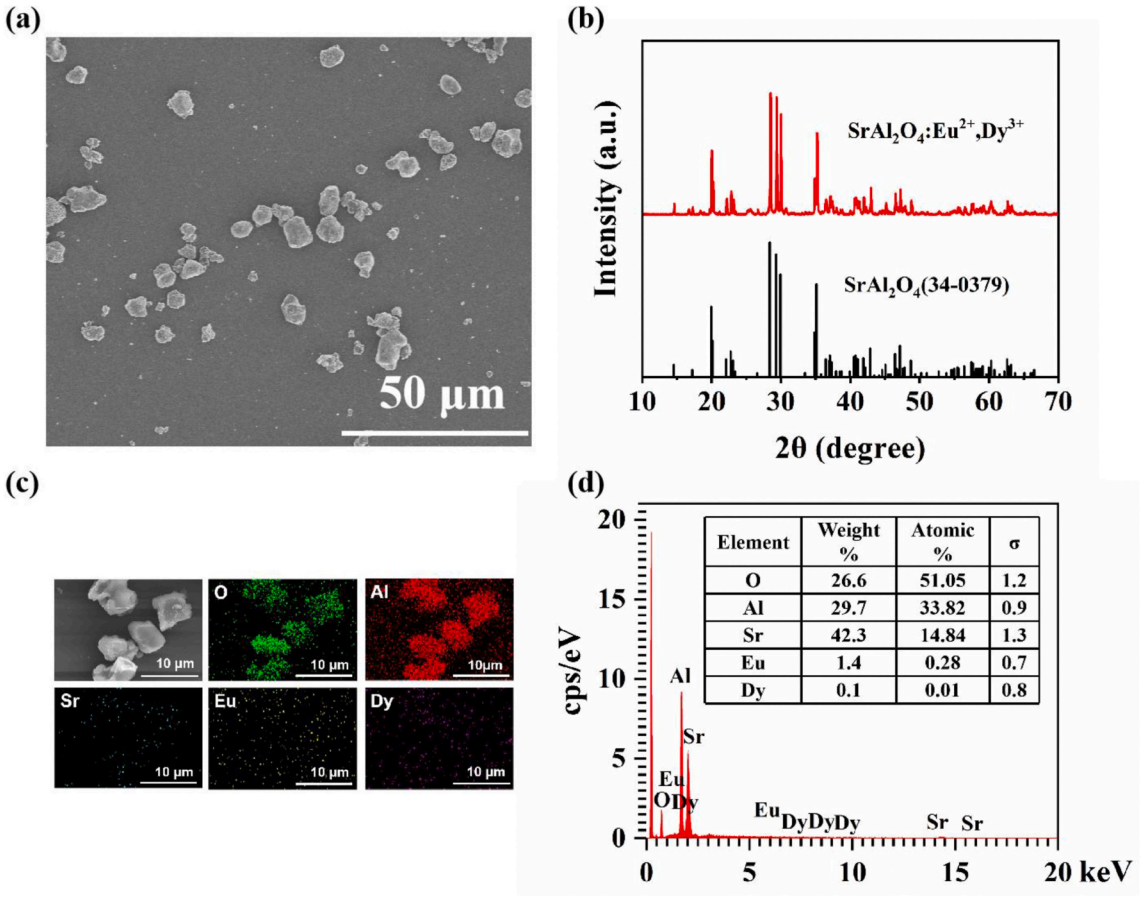


**Fig. 2.** (a) SEM image, (b) XRD patterns, (c) elemental mapping and (d) EDS of APs.

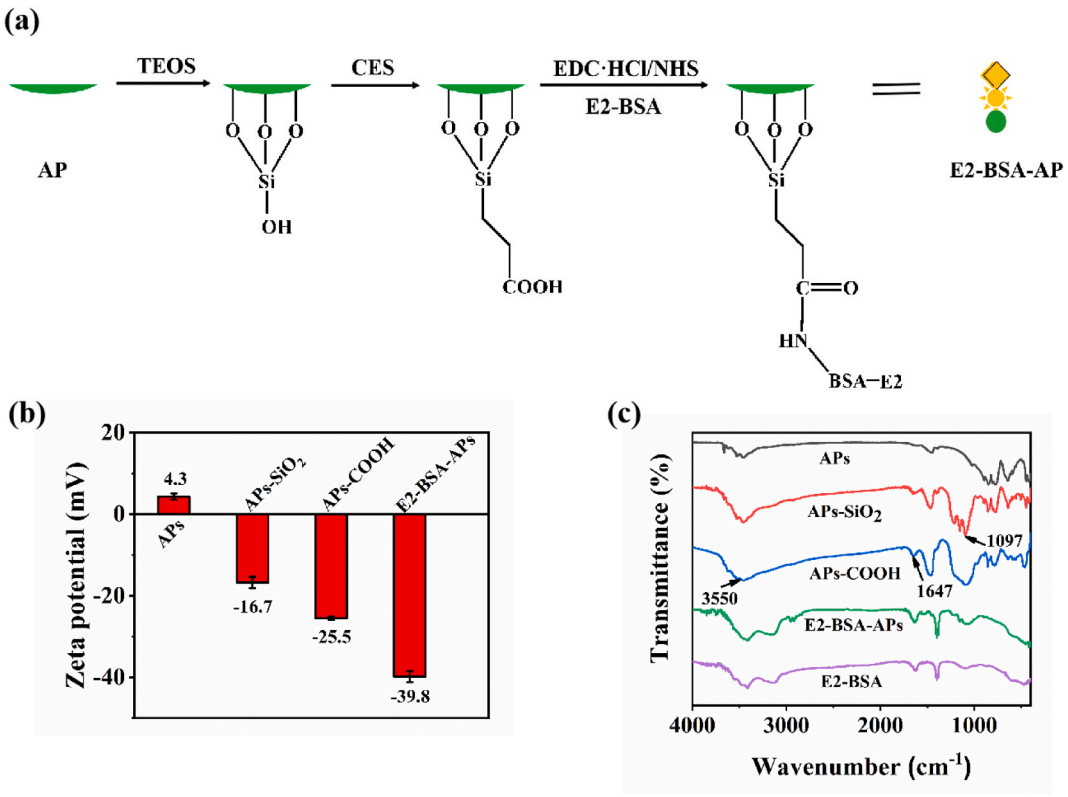


**Fig. 3.** (a) Mechanism of E2-BSA-AP synthesis, (b) Zeta potentials and (c) FT-IR spectra of APs and modified APs.

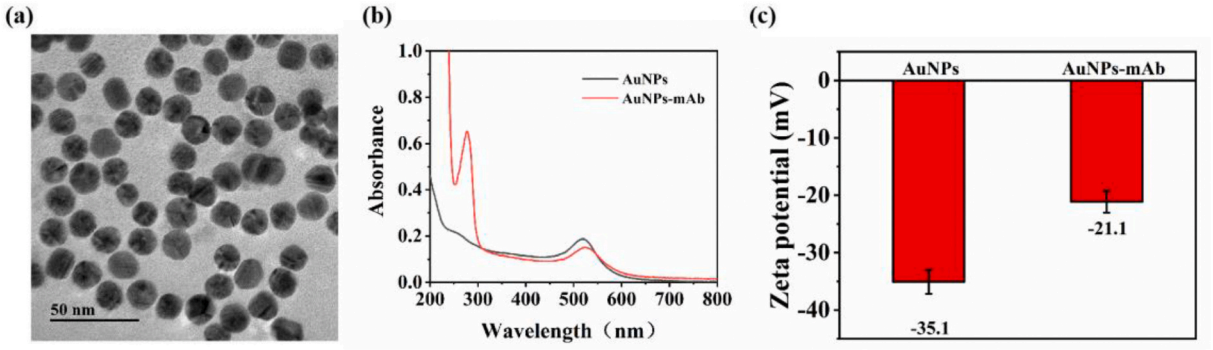


**Fig. 4.** Characterization of AuNPs and AuNPs-mAb. (a) TEM image of AuNPs. The UV–vis absorption spectra (b) and zeta potentials of AuNPs and AuNPs-mAb (c).

keep lighting for more than 20 min, demonstrating that they possess great afterglow character (Fig. 5b). There was neither visible APs at the front of the flowing liquid nor obvious change in the afterglow brightness and the spot size at the spotting position after running buffer flushing the NC membrane, indicating these APs could not migrate through NC membrane but stayed at the spotting position because they were too large to run (Fig. 5b inset).

As shown in Fig. 5c, the emission spectrum of APs overlaps with the absorption spectrum of AuNPs to a large extent, satisfying one of the necessary conditions for FRET: spectra overlap between energy donor and acceptor. These optical characters of APs and AuNPs make the FRET-based dual-mode ICS feasible.

### 3.4. Optimization of the ICS assay

We optimized the amount of AuNPs-mAb and E2-BSA-APs according to the T-zone signal intensity of negative sample in both visual and afterglow detection modes and the images were analyzed in the grayscale mode by ImageJ software. In the visual mode, the red color on T zone gradually increases with the dosage rise of AuNPs-mAb and E2-BSA-APs, whereas there is no obvious difference between group of E2-BSA-APs of 2 mg/mL and 4 mg/mL (Fig. 6a). Thus, the dosage of AuNPs-mAb should be 2 μL or above and that of E2-BSA-APs should be 2 mg/mL or above to give a clear and bright red color at T zone for negative samples in visual detection mode. In the afterglow mode (Fig. 6b), the afterglow of APs should be quenched thoroughly by AuNPs for negative samples, but it is not the case when the concentration of E2-BSA-APs is 4 mg/mL. Therefore, considering the results of both modes, when the dosage of E2-BSA-APs is 2 mg/mL and that of AuNPs-mAb is 5 μL, we can get both clear visual and well quenched afterglow signals for negative samples.

To realize time control and improve the sensitivity, the excitation time and the capture time of afterglow was optimized by analyzing the afterglow intensity at T zone of ICS images taken by a smartphone in continuous shooting mode (Fig. 6c and d). The smart phone we used takes 20 photos continuously in 2 s after clicking shott button under

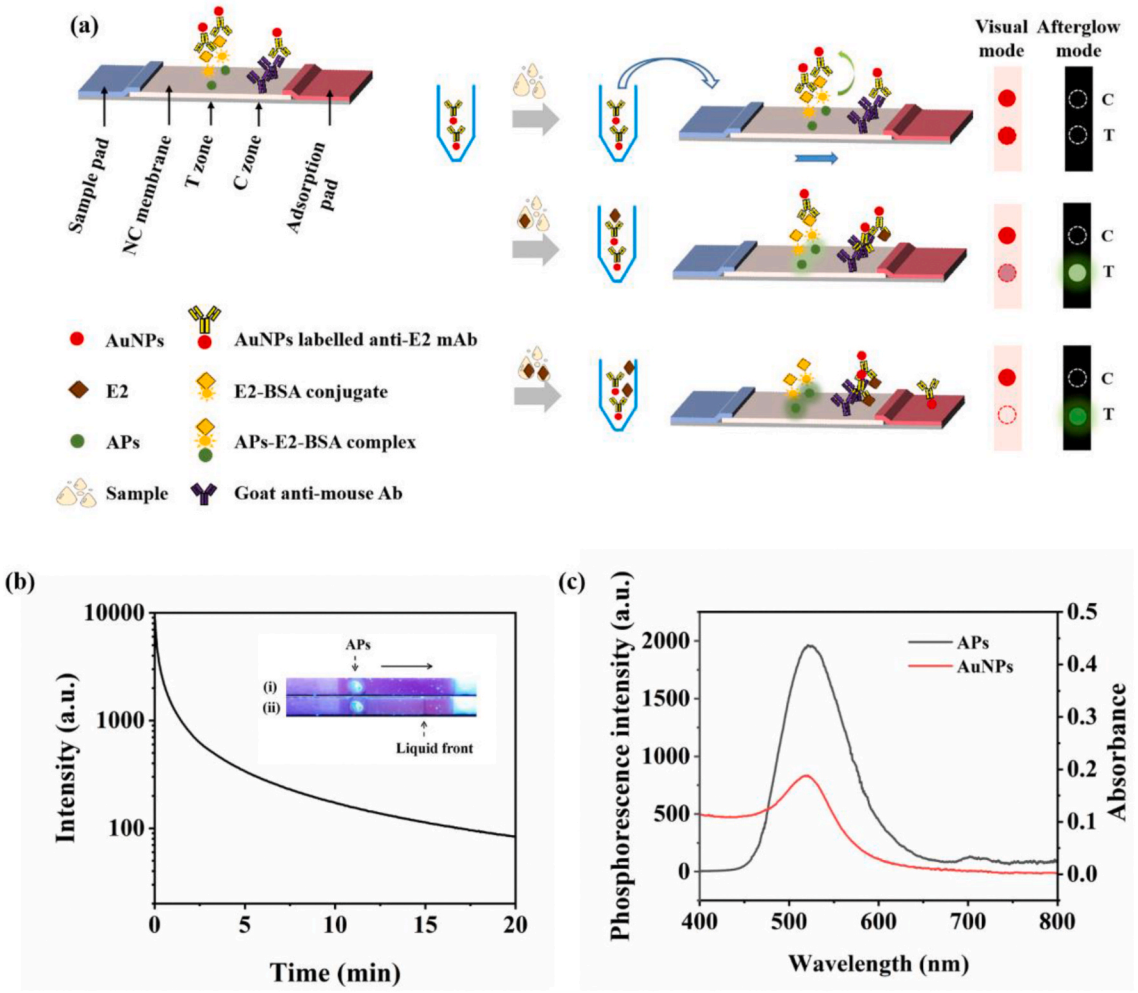


**Fig. 5.** (a) Schematic depiction of the setups for visual-afterglow dual-mode ICSs for the detection of E2. (b) Luminescence decay curve of APs after a 3 min excitation under a 254 nm UV light. Inset. Strip photos under UV light (i) before and (ii) after running buffer flushing. (c) Absorbance spectrum of AuNPs and emission spectrum of APs.

continuous shooting mode, indicating a time gap of 0.1 s between each two adjacent photos. We sequenced the photos in captured time, and named the first photo after the UV-lamp went out as "0.1 s", then "0.2 s", "0.3 s", and so on. We compared the afterglow intensity at test-zone of negative and positive samples ([E2] = 10 ng/mL) and selected "0.5 s" as the optimal one because it gave a bright enough positive signal and a negligible negative signal. Although there is a huge decrease of intensity in the afterglow decay curve for the first seconds, according to the statistics of the decay afterglow intensity decay occurs at a rate of only 5%–6% every 0.5 s initially, which is within the acceptable range. Thus, the afterglow image capture time was set as 0.5 s.

### 3.5. Assessment of ICS sensitivity and specificity

The sensitivity of developed ICS was analyzed in both visual and afterglow mode. In afterglow detection mode, the afterglow of T zone lighted up at E2 of 0.5 ng/mL and turned brighter at higher concentrations, indicating the limit of detection (LOD) of E2 in afterglow detection mode is 0.5 ng/mL (Fig. 7b). In visual detection mode, the red color of T zone faded slightly at E2 of 5 ng/mL and disappeared thoroughly at E2 of 10 ng/mL (Fig. 7a). In this study, the threshold E2 concentration was defined as the cutoff value when the T zone disappeared, which is also taken as the LOD of E2 in visual mode. Therefore the LOD of E2 in visual mode is 10 ng/mL, 20 times higher than in afterglow mode, demonstrating the superiority of afterglow mode in sensitivity.

Some ICS methods for E2 detection were compared in Table 1. In addition to AuNPs, the label materials included novel $Fe_3O_4$ magnetic nanoparticles (MNP), black phosphorescence (BP) and graphite-like carbon nitride g-$C_3N_4$. These new probes were more sensitive than AuNPs. This work introduced APs to develop FRET-ICS and obtained good sensitivity by improving signal-to-noise ratio.

The specificity of the dual-mode ICS was assessed by testing four analogues of E2 (Table 2). Being consistent with the result of sensitivity, E2 of 10 ng/mL gave a positive in both visual and afterglow modes. E1, BPA and DES up to 100 ng/mL didn't change the signal obviously on T zone in both modes. However, E3 of 100 ng/mL in visual mode, and E3 of 20 ng/mL in afterglow mode also gave a weak positive, possibly due to the greater similarity in chemical structures of E2 and E3. These results indicated high specificity of our dual-mode ICS toward E2.

### 3.6. Samples analysis

To evaluate the validity of this method, milk samples spiked with E2 were analyzed by the developed dual-mode ICS. Liquid chromatography is widely used as standard analytical method to validate other new analytical methods and our analyte E2 could be detected by fluorescence detector. Therefore, HPLC-FLD was used to validate the results of our dual-mode ICS. The prepared sample solutions were spiked with E2 to obtain a series of concentrations including 0 ng/mL, 1 ng/mL and 10 ng/

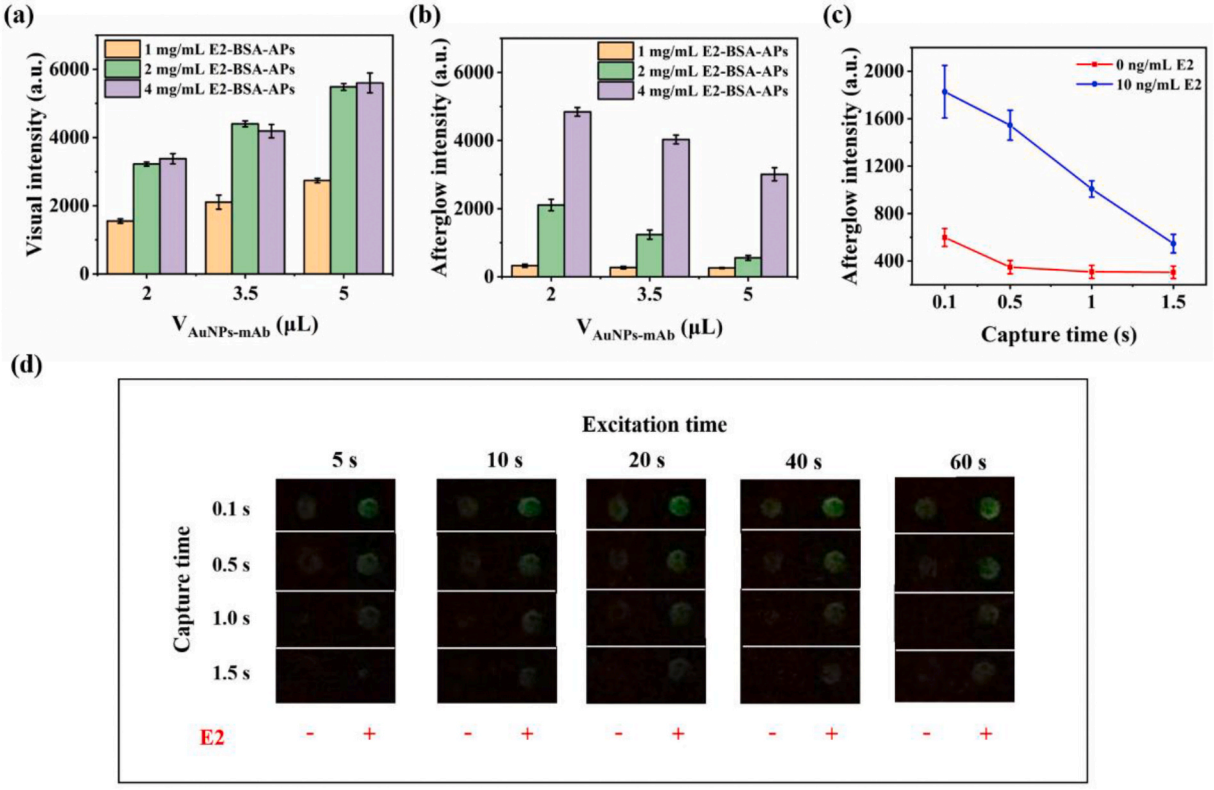


**Fig. 6.** The effects of E2-BSA-APs dosage and AuNPs-mAb dosage on the signal intensity of (a) visual mode and (b) afterglow mode, respectively, E2 at 0 ng/mL. The effects of excitation time and capture time on the signal intensity of afterglow mode, (c) and (d), E2 at 0 ng/mL (−) or 10 ng/mL (+).

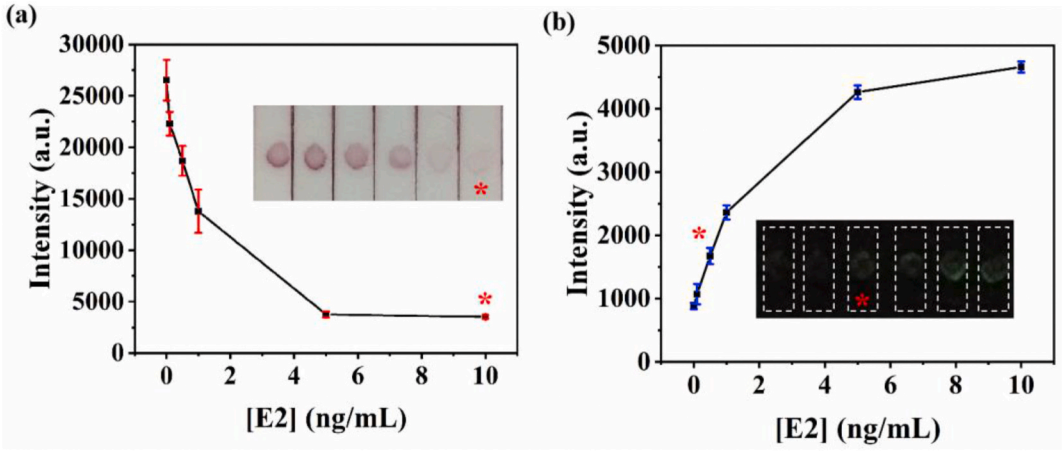


**Fig. 7.** E2 detection by the visual (a) and afterglow (b) ICS.

mL. The red color of T zone disappeared at 10 ng/mL E2 in visual mode, and the afterglow of T zone was observed at 1 ng/mL and above. E2 recoveries were 103.1%–109.4% from HPLC–FLD for samples spiked with 10 ng/mL, but no E2 was detected for samples spiked with 1 ng/mL. These results were analyzed in Table 3. The dual-mode ICS assay allows a semiquantitative determination of E2 and the results obtained from the dual-mode ICS were consistent with those obtained from HPLC–FLD.

## 4. Conclusions

In this study, a dual-mode ICS strategy was developed to detect E2 in milk. We achieved a positively correlated signal-[analyte] relationship and a more sensitive E2 detection with relatively low background via the FRET-based afterglow mode. The contradiction between migration and afterglow characteristics of APs, which limit the application of micron-sized APs in ICS, has been addressed by fixing them at test zone rather than flushing them through the membrane. Smartphone was used to capture afterglow under continuous shooting mode to implement time control in an easy-to-run way. The sensitivity of afterglow mode was twenty times higher than that of visual mode. We applied this method to detect E2 in spiked milk. The results were consistent with those obtained from HPLC–FLD, and the afterglow mode was proved to be more sensitive than visual mode and HPLC–FLD. Therefore, this dual-mode ICS can be used as a combination of the fast visual screen and the sensitive afterglow detection for detecting E2 in milk.

**Table 1**
Comparison of the detection performance of our dual-mode ICS and other similar methods.

| Format | Probe | LOD or cutoff value (ng/mL) | Detection time (min) | Ref |
|---|---|---|---|---|
| Traditional | AuNPs | 50 | 10 | [10] |
| Traditional | AuNPs | 5 | 10–15 | [11] |
| Traditional | g-$C_3N_4$@AuNPs | 10 | 10 | [34] |
| Traditional | MNP | 30 | 10 | [35] |
| Dual probe | MNP | 10 | 10 | [35] |
| Indirect probe | MNP | 5 | 10 | [35] |
| Traditional | BP | 0.104 | 15 | [36] |
| Dual-mode | AuNPs, APs | 0.5 (APs), 10 (AuNPs) | 20 | This work |

**Table 2**
The selectivity of the dual-mode ICS.

| Chemicals | E2 | E1 | E3 | BPA | DES |
|---|---|---|---|---|---|
| Visual detection mode | <10[a] | >100 | ~100 | >100 | >100 |
| Afterglow detection mode | <1[b] | >100 | ~10 | >100 | >100 |

[a] Cut-off value (ng/mL).
[b] Afterglow light-up.

**Table 3**
Analysis of E2 in milk samples by HPLC–FLD and dual-mode ICS (n = 3).

| Samples | Spiked (ng/mL) | HPLC–FLD | | Dual-mode ICS | |
|---|---|---|---|---|---|
| | | Detected (Mean ± SD, ng/mL) | Recovery (%) | Visual mode | Afterglow mode |
| Milk 1 | 0 | ND[a] | NC[b] | − − −[c] | − − − |
| | 1 | ND | NC | − − − | + + +[d] |
| | 10 | 10.94 ± 0.11 | 109.4 ± 1.1 | + + + | + + + |
| Milk 2 | 0 | ND | NC | − − − | − − − |
| | 1 | ND | NC | − − − | + + + |
| | 10 | 10.31 ± 0.74 | 103.1 ± 7.4 | + + + | + + + |
| Milk 3 | 0 | ND | NC | − − − | − − − |
| | 1 | ND | NC | − − − | + + + |
| | 10 | 10.63 ± 0.63 | 106.3 ± 6.4 | + + + | + + + |

[a] ND, not detected.
[b] NC, not calculated.
[c] −, negative, the concentration of E2 was <0.5 ng/mL.
[d] +, positive, the concentration of E2 was ≥0.5 ng/mL.

## Credit author statements

Yi Zhang supplied critical suggestions, wrote and revised the manuscript. Lingling Wang did most of the experimental work, analyzed the data and wrote the manuscript. Wen-Long Wang guided the experiment process and supplied critical suggestions. Cheng Yang did the HPLC and ESI-MS measurements. Yongwei Feng and Xueli Shi revised the manuscript. And all authors have reviewed the manuscript.

## Declaration of competing interest

The authors declare that they have no known competing financial interests or personal relationships that could have appeared to influence the work reported in this paper.

## Acknowledgements

This work was supported by the National Natural Science Foundation of China (21876066), National First-Class Discipline Program of Food Science and Technology (JUFSTR20180301), Science and Technology Project of Jiangsu Market Supervision Administration (KJ204131) and Hebei Medical Science Research Project (20212039, 20211856).

## References

[1] M. Adeel, X. Song, Y. Wang, D. Francis, Y. Yang, Environmental impact of estrogens on human, animal and plant life: a critical review, Environ. Int. 99 (2017) 107–119, https://doi.org/10.1016/j.envint.2016.12.010.
[2] T.T. Schug, A. Janesick, B. Blumberg, J.J. Heindel, Endocrine disrupting chemicals and disease susceptibility, J. Steroid Biochem. Mol. Biol. 127 (2011) 204–215, https://doi.org/10.1016/j.jsbmb.2011.08.007.
[3] X. Tian, H. Song, Y. Wang, X. Tian, Y. Tang, R. Gao, C. Zhang, Hydrophilic magnetic molecularly imprinted nanobeads for efficient enrichment and high performance liquid chromatographic detection of 17beta-estradiol in environmental water samples, Talanta 220 (2020) 121367, https://doi.org/10.1016/j.talanta.2020.121367.
[4] A.A. Paria, T. Zahra, F. Lida, Introduction of electropolymerization of pyrrole as a coating method for stir bar sorptive extraction of estradiol followed by gas chromatography, J. Chromatogr. A 1604 (2019) 460478, https://doi.org/10.1016/j.chroma.2019.460478.
[5] Q. Han, X. Shen, W. Zhu, C. Zhu, X. Zhou, H. Jiang, Magnetic sensing film based on $Fe_3O_4$@Au-GSH molecularly imprinted polymers for the electrochemical detection of estradiol, Biosens. Bioelectron. 79 (2016) 180–186, https://doi.org/10.1016/j.bios.2015.12.017.
[6] R. Wang, H. Chou, S. Lee, Z. Cheng, S.H. Hong, Y.H. Yoon, J. Choo, Highly sensitive detection of hormone estradiol E2 using surface-enhanced Raman scattering based immunoassays for the clinical diagnosis of precocious puberty, ACS Appl. Mater. Interfaces 8 (2016) 10665–10672, https://doi.org/10.1021/acsami.5b10996.
[7] P.Y. You, F.C. Li, M.H. Liu, Y.H. Chan, Colorimetric and fluorescent dual-mode immunoassay based on plasmon-enhanced fluorescence of polymer dots for detection of PSA in whole blood, ACS Appl. Mater. Interfaces 11 (2019) 9841–9849, https://doi.org/10.1021/acsami.9b00204.
[8] B. Jin, Y. Yang, R. He, Y. ll Park, A. Lee, D. Bai, F. Li, T.J. Lu, F. Xu, M. Lin, Lateral flow aptamer assay integrated smartphone-based portable device for simultaneous detection of multiple targets using upconversion nanoparticles, Sensor. Actuator. B Chem. 276 (2018) 48–56, https://doi.org/10.1016/j.snb.2018.08.074.
[9] M. Xiao, Q. Fu, H. Shen, Y. Chen, W. Xiao, D. Yan, X. Tang, Z. Zhong, Y. Tang, A turn-on competitive immunochromatographic strips integrated with quantum dots and gold nano-stars for cadmium ion detection, Talanta 178 (2018) 644–649, https://doi.org/10.1016/j.talanta.2017.10.002.
[10] Z. Xu, T. Sun, H. He, W. Liu, L. Fan, L. Zhao, X. Wu, Zh Han, Y. Zhang, Q. Wang, B. Ning, Z. Gao, Simultaneous detection of diethylstilbestrol and estradiol residues with a single immunochromatographic assay strip, Food Sci. Nutr. 9 (2021) 1824–1830, https://doi.org/10.1002/fsn3.2127.
[11] Z. Wang, L. Guo, L. Liu, H. Kuang, C. Xu, Colloidal gold-based immunochromatographic strip assay for the rapid detection of three natural estrogens in milk, Food Chem. 259 (2018) 122–129, https://doi.org/10.1016/j.foodchem.2018.03.087.
[12] X. Yang, F. Wang, C. Song, S. Wu, G. Zhang, X. Zeng, Establishment of a lateral flow colloidal gold immunoassay strip for the rapid detection of estradiol in milk samples, LWT - Food Sci. Technol. (Lebensmittel-Wissenschaft -Technol.) 64 (2015) 88–94, https://doi.org/10.1016/j.lwt.2015.04.022.
[13] X. Li, X. Wu, J. Wang, Q. Hua, J. Wu, X. Shen, Y. Sun, H. Lei, Three lateral flow immunochromatographic assays based on different nanoparticle probes for on-site detection of tylosin and tilmicosin in milk and pork, Sensor. Actuator. B Chem. 301 (2019) 127059, https://doi.org/10.1016/j.snb.2019.127059.
[14] X. Huang, Z.P. Aguilar, H. Xu, W. Lai, Y. Xiong, Membrane-based lateral flow immunochromatographic strip with nanoparticles as reporters for detection: a review, Biosens. Bioelectron. 75 (2016) 166–180, https://doi.org/10.1016/j.bios.2015.08.032.
[15] R. Tang, H. Yang, J.R. Choi, Y. Gong, J. Hu, S. Feng, B. Pingguan-Murphy, Q. Mei, F. Xu, Improved sensitivity of lateral flow assay using paper-based sample concentration technique, Talanta 152 (2016) 269–276, https://doi.org/10.1016/j.talanta.2016.02.017.
[16] R. Yin, Y. Sun, K. Wang, N. Feng, H. Zhang, M. Xiao, Development of a PCR-based lateral flow strip assay for the simple, rapid, and accurate detection of pork in meat and meat products, Food Chem. 318 (2020), 126541, https://doi.org/10.1016/j.foodchem.2020.126541.
[17] L. Hao, J. Chen, X. Chen, T. Ma, X. Cai, H. Duan, Y. Leng, X. Huang, Y. Xiong, A novel magneto-gold nanohybrid-enhanced lateral flow immunoassay for ultrasensitive and rapid detection of ochratoxin A in grape juice, Food Chem. 336 (2020), https://doi.org/10.1016/j.foodchem.2020.127710, 127710-127710.
[18] I.N. Katis, P.J.W. He, R.W. Eason, C.L. Sones, Improved sensitivity and limit-of-detection of lateral flow devices using spatial constrictions of the flow-path, Biosens. Bioelectron. 113 (2018) 95–100, https://doi.org/10.1016/j.bios.2018.05.001.
[19] Q.-G. Daniel, S. Christina, G. Israel, E.-M. Alfredo Escosura-Muñiz, D. Neus, M. Pere, M. Arben, Signal enhancement on gold nanoparticle-based lateral flow tests using cellulose nanofibers, Biosens. Bioelectron. 141 (2019) 111407, https://doi.org/10.1016/j.bios.2019.111407.
[20] Y. Wang, X. Zhao, M. Zhang, X. Sun, J. Bai, Y. Peng, S. Li, D. Han, S. Ren, J. Wang, T. Han, Y. Gao, B. Ning, Z. Gao, A fluorescent amplification strategy for high-

sensitive detection of 17β-estradiol based on EXPAR and HCR, Anal. Chim. Acta 1116 (2020) 1–8, https://doi.org/10.1016/j.aca.2020.04.010.
[21] L.-M. Hu, K. Luo, J. X, G.-M. Xu, C.-H. Wu, J.-J. Han, G.-G. Zhang, M. Liu, W.-H. Lai, Advantages of time-resolved fluorescent nanobeads compared with fluorescent submicrospheres, quantum dots, and colloidal gold as label in lateral flow assays for detection of ractopamine, Biosens. Bioelectron. 91 (2017) 95–103, https://doi.org/10.1016/j.bios.2016.12.030.
[22] M. Majdinasab, M. Zareian, Q. Zhang, P. Li, Development of a new format of competitive immunochromatographic assay using secondary antibody–europium nanoparticle conjugates for ultrasensitive and quantitative determination of ochratoxin A, Food Chem. 275 (2019) 721–729, https://doi.org/10.1016/j.foodchem.2018.09.112.
[23] H. Deng, Q. Liu, X. Wang, R. Huang, H. Liu, Q. Lin, X. Zhou, D. Xing, Quantum dots-labeled strip biosensor for rapid and sensitive detection of microRNA based on target-recycled nonenzymatic amplification strategy, Biosens. Bioelectron. 87 (2017) 931–940, https://doi.org/10.1016/j.bios.2016.09.043.
[24] X. Deng, C. Wang, Y. Gao, J. Li, W. Wen, X. Zhang, S. Wang, Applying strand displacement amplification to quantum dots-based fluorescent lateral flow assay strips for HIV-DNA detection, Biosens. Bioelectron. 105 (2018) 211–217, https://doi.org/10.1016/j.bios.2018.01.039.
[25] M. Yang, Y. Zhang, M. Cui, Y. Tian, S. Zhang, K. Peng, H. Xu, Z. Liao, H. Wang, J. Chang, A smartphone-based quantitative detection platform of mycotoxins based on multiple-color upconversion nanoparticles, Nanoscale 10 (2018) 15865–15874, https://doi.org/10.1039/c8nr04138e.
[26] B. Jin, Y. Yang, R. He, Y. II Park, A. Lee, D. Bai, F. Li, T.J. Lu, F. Xu, M. Lin, Lateral flow aptamer assay integrated smartphone-based portable device for simultaneous detection of multiple targets using upconversion nanoparticles, Sensor. Actuator. B Chem. 276 (2018) 48–56, https://doi.org/10.1016/j.snb.2018.08.074.
[27] Y. Li, Mi Geceviciusa, J. Qiu, Long persistent phosphors—from fundamentals to applications, Chem. Soc. Rev. 45 (2016) 2090, https://doi.org/10.1039/c5cs00582e.
[28] A.S. Paterson, B. Raja, G. Garvey, A. Kolhatkar, A.E.V. Hagström, K. Kourentzi, T. R. Lee, R.C. Willson, Persistent luminescence strontium aluminate nanoparticles as reporters in lateral flow assays, Anal. Chem. 86 (2014) 9481–9488, https://doi.org/10.1021/ac5012624.
[29] A.S. Paterson, B. Raja, V. Mandadi, B. Townsend, M. Lee, A. Buell, B. Vu, J. Brgoch, R.C. Willson, A low-cost smartphone-based platform for highly sensitive point-of-care testing with persistent luminescent phosphors, Lab Chip 17 (2017) 1051–1059, https://doi.org/10.1039/c6lc01167e.
[30] A.N. Danthanarayana, E. Finley, B. Vu, K. Kourentzi, R.C. Willson, J. Brgoch, A multicolor multiplex lateral flow assay for high-sensitivity analyte detection using persistent luminescent nanophosphors, Anal. Methods 12 (2020) 272–280, https://doi.org/10.1039/c9ay02247c.
[31] B.-Y. Wu, X.-P. Yan, Bioconjugated persistent luminescence nanoparticles for Föster resonance energy transfer immunoassay of prostate specific antigen in serum and cell extracts without in situ excitation, Chem. Commun. 51 (2015) 3903–3906, https://doi.org/10.1039/c5cc00286a.
[32] L.N. Dou, B.X. Zhao, T. Bu, W.T. Zhang, Q. Huang, L.Z. Yan, L.J. Huang, Y.R. Wang, J.L. Wang, D.H. Zhang, Highly sensitive detection of a small molecule by a paired labels recognition system based lateral flow assay, Anal. Bioanal. Chem. 410 (2018) 3161–3170, https://doi.org/10.1007/s00216-018-1003-0.
[33] V. Vitola, D. Millers, I. Bite, K. Smits, A. Spustaka, Recent progress in understanding the persistent luminescence in SrAl2O4: Eu, Dy, Mater, Sci. Technol. 35 (2019) 1661–1677, https://doi.org/10.1080/02670836.2019.1649802.
[34] X. Yao, Z. Wang, Ma Zhao, S. Liu, L. Su, L. Dou, T. Li, J. Wang, D. Zhang, Graphite-like carbon nitride-laden gold nanoparticles as signal amplification label for highly sensitive lateral flow immunoassay of 17β-estradiol, Food Chem. 347 (2021) 129001, https://doi.org/10.1016/j.foodchem.2021.129001.
[35] X. Yao, Z. Wang, L. Dou, B. Zhao, Y. He, J. Wang, J. Sun, T. Li, D. Zhang, An innovative immunochromatography assay for highly sensitive detection of 17β-estradiol based on an indirect probe strategy, Sensor. Actuator. B Chem. 289 (2019) 48–55, https://doi.org/10.1016/j.snb.2019.03.078.
[36] L. Lu, M. Wang, D. Zhang, H. Zhang, Establishment of an immunofiltration strip for the detection of 17β-estradiol based on the photothermal effect of black phosphorescence, Analyst 144 (2019) 6647–6652, https://doi.org/10.1039/c9an01495.